ELSEVIER

Chemical Engineering Journal 77 (2000) 65–72

Chemical Engineering Journal

www.elsevier.com/locate/cej

X-ray computer tomography — potential and limitation for the measurement of local solids distribution in circulating fluidized beds

T. Grassler *, K.-E. Wirth

Lehrstuhl fuer Mechanische Verfahrenstechnik, Universitaet Erlangen-Nuernberg, Cauerstrasse 4, 91058 Erlangen, Germany

Abstract

The characterization of the gas–solids flow inside a circulating fluidized bed, especially the knowledge about the solids distribution in the vertical tubes, is the basis for a optimum reactor design as well as for finding suitable operating conditions and for modeling the multiphase flow inside the reactor. To determine data of solids concentration with high spatial resolution an X-ray computer tomography system is used. This system mainly consists of a 60 keV X-ray source and an X-ray linear detector with 1024 sensitive elements, which gives eight bit-values representing integral solids concentrations between the X-ray source and the detector. A number of experiments have been carried out both at the upflow and at the downflow of two different circulating fluidized beds containing glass beads of 70 μm at superficial gas velocities from 2 to 7 m/s. Results show that the X-ray computer tomography system is applicable to average solids concentrations from 1 up to 20 vol% of solids concentration in a tube with 0.19 m inner diameter.

Keywords: X-ray; Computer tomography; Circulating fluidized bed; Multiphase flow

1. Introduction

In chemical and process industry vertical multiphase flows play an important role in different fields from processing chemicals and fuel to the production of pharmaceuticals, food and a lot of specialty materials. The characterization of the multiphase flow inside such reactors, especially the knowledge about the concentration distribution in the vertical tube, is the basis for technical constructions.

In the field of process engineering a trend towards simulation and calculation of fluid dynamics and heat transfer can be observed. Such models require accurate data with high spatial resolution, which cannot be obtained by most of the commonly used measurement techniques.

In most of the studies, concerned with characterizing flow patterns in circulating fluidized beds, concentration distributions are calculated from vertical pressure gradients or measured with various kinds of intrusive probes [1–3]. However, pressure drop profiles only lead to integral values of concentration along a certain length of the tube, if acceleration and deceleration effects are neglected. By using probes a disturbance of the gas–solids flow can never be excluded and often a large-scale calibration is necessary. Moreover, the spatial resolution of probes is poor and only single points of the whole measuring area can be detected at a certain time.

Additionally to these conventional measuring techniques to characterize the solids concentration distribution in circulating fluidized beds [4] also describe non-intrusive imaging techniques like X-ray or γ-ray attenuation. Systems based on X-ray attenuation have been presented for example by [5] or [6]. With the equipment used the turbulence of fluidized beds has been studied by taking ‘instantaneous’ snapshots with a time resolution of up to 45 frames/s. These snapshots are taken from one fixed position so radial symmetry of the flow structures is necessary to calculate the local solids concentration. However, the solids concentration distribution can be asymmetric especially near the inlet or exit of a circulating fluidized bed. In order to study also asymmetric concentration distributions tomographic measuring techniques with snapshots from different angular positions are necessary.

Therefore, an X-ray computer tomography system has been developed as a non-intrusive technique with high spatial resolution to determine the local solids concentration in the tube cross section of vertical tubes used in pneumatic conveying or circulating fluidized beds.

Tomographic measurements have been carried out at different elevations of two cold-running circulating fluidized beds in a technical scale, both at the upflow and at the downflow. Results from the circulating fluidized beds together with measurements of well-defined objects made of plexiglas show the potential and the limits of such a tomographic system in process engineering.

* Corresponding author. Tel.: +49-9131-8529400.
E-mail address: sekretariat@mvt.uni-erlangen.de (T. Grassler).

1385-8947/00/$ – see front matter
PII: S1385-8947(99)00133-3

Nomenclature

c	velocity of light $= 2.99792 \times 10^8$ (m/s)
e	electronic charge $= 1.6022 \times 10^{-19}$ (C)
E	energy of X-ray (eV)
g	gravitational acceleration $= 9.80665$ (m^2/s)
h	height of the riser facility (m)
h	Planck's constant $= 6.6262 \times 10^{-34}$ (Js)
I	X-ray intensity, transmission
I_0	intensity of the X-ray source
L	thickness of absorbing material (m)
G_S	specific solids mass flux (kg/(m^{2}s))
s	coordinate along an X-ray beam (m)
U_G	superficial gas velocity (m/s)
V_0	high voltage applied to the X-ray tube (V)
Z	atomic number
ε	porosity
$1-\varepsilon$	solids volume fraction
λ	wavelength (m)
λ_0	cutoff wavelength (m)
μ	linear absorption coefficient (1/m)
ρ	density of material (kg/m^3)

2. Principle of X-ray computer tomography

Computer tomography is a technology, that allows the non-destructive evaluation of the internal structure of objects. Since many years this technique has been used successfully in medicine and material testing to examine local differences in density by generating images of different cutting planes of the object concerned. Recently, some efforts have been made to use γ-ray and X-ray computer tomography in multiphase flows [7,8,9,10].

Computer tomography systems consist of two main parts, namely a physical measuring technique, which yields to integral values of the wanted local variable along certain paths, and a mathematical reconstruction algorithm, which calculates the local concentrations from the obtained raw data. In literature a lot of physical sensing methods, available for tomographic measurements, and as well a great number of possible reconstruction techniques can be found [11]. The physical measuring system to obtain the distributions of local solids concentration presented in this paper consists of an X-ray source and an X-ray linear detector to measure the attenuation along a multitude of ray paths through the sample. These data are reconstructed by an algebraic reconstruction technique (ART) [12,13], which is the most common algorithm for industrial applications with limited measurement information.

Instead of γ-ray or X-ray tomography systems recently capacitance tomography is used to determine the local solids concentration distribution in gas–solids flows [21,22]. These systems provide a very high time resolution of up to 200 frames/s but very poor spatial resolution in the range of centimeters. Moreover, a strenuous calibration and reconstruction procedure is necessary to get sufficient results.

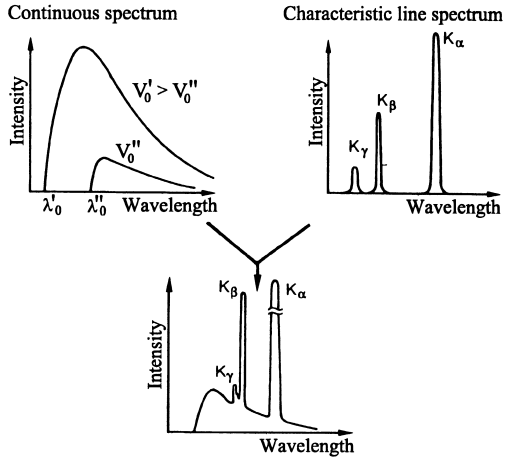

Fig. 1. Schematic emissions spectrum of an X-ray source [16].

2.1. Energy spectrum of X-rays

X-rays for technical purposes are normally produced in an X-ray tube. Electrons emitted from a cathode which is heated by a filament are accelerated toward the anode by high voltage between the two electrodes. When the electrons hit the anode, designated as target, they are decelerated which is accompanied by emission of electromagnetic radiation. The emission spectrum of an X-ray tube consists of a continuous spectrum and a characteristic line spectrum.

Wavelength characteristics of the resulting continuous spectrum are completely independent of the target material and depend only on the voltage, V_0, applied to the X-ray tube [14]. The higher the voltage, the shorter the minimum or cutoff wavelength produced (see Fig. 1). The cutoff wavelength, λ_0, can be calculated by the following empirical equation, where h is the Planck's constant, c the velocity of light and e represents the electronic charge:

$$\lambda_0 = \frac{hc}{eV_0} \quad \text{with} \quad \frac{hc}{e} = 1.24 \times 10^{-6}\,\text{m V} \tag{1}$$

The spectral intensity distribution I of the electromagnetic radiation as a function of the wavelength, λ, can be approximately calculated from [15]:

$$I(\lambda) = \frac{\lambda - \lambda_0}{\lambda^3 \lambda_0} \tag{2}$$

Eq. (2) gives the spectral intensity in any dimensions and represents only the shape of the continuous spectrum.

In addition to that continuous spectrum sharp lines occur in the X-ray region of the spectrum. These lines are superimposed on the continuous X-ray spectrum and can be explained on the basis of the simple Bohr theory. In the target electrons can be removed from the atom by electron collision processes. Then electrons from outer shells can fall into the

gap which produces characteristic radiation. This process is strongly influenced by the pattern of the electron sheath and therefore by the material of the target. The addition of the continuous spectrum and the characteristic line spectrum to the whole X-ray spectrum is shown in Fig. 1 on principle.

2.2. Interaction of X-rays with material

If X-rays pass through an object, the original spectral intensity distribution is influenced, depending on the material and the thickness of the object. The irradiation of an infinitesimal thin layer of material ds with a monoenergetic parallel beam causes a decrease in the intensity dI of the radiation, which depends on the linear absorption coefficient of the material μ:

$$\mathrm{d}I = -I\mu\,\mathrm{d}s \tag{3}$$

With integrating over the whole thickness L of the object the residual intensity I of an original intensity I_0 can be calculated:

$$I = I_0 \mathrm{e}^{-\mu L} \tag{4}$$

In practice, the linear absorption coefficient μ is no matter constant, but depends on the spectral intensity distribution of the radiation source, the density ρ and the atomic number Z of the object. The reason for the decrease in intensity of the X-ray by penetrating material are three different effects: photoelectric effect; scattering (coherent, incoherent); and pair production [17].

- Photoelectric effect and Auger effect: an X-ray quantum hits an electron of the electronic sheath with enough energy to remove this electron. The atom returns to a state of lower energy by filling the hole with an electron from an outer shell and by simultaneously emitting an electromagnetic quantum. If this quantum hits an electron in an outer shell so that the electron is removed, the process is called Auger effect.
- Coherent scattering: when a beam of X-rays passes an electron of the electronic shell, part of it is scattered into a spherical wave diverging from the location of the electron. X-ray quantums are diffracted from their original direction with retention of their energy.
- Incoherent scattering or Compton effect: when a relatively hard X-ray quantum is scattered by an electron, it partially loses energy to the scattering electron.
- Pair production: if the energy of a quantum is >1.022 MeV, it may be absorbed in the field of an atomic nucleus with the creation or generation of an electron–positron pair. The quantum energy is partly converted into the rest energy of the two created particles, the excess going into their kinetic energy.

The linear absorption coefficient μ can be calculated by adding the extinction coefficients of the different processes of attenuation described above. Fig. 2 shows these linear absorption coefficients divided by the material density for the above-mentioned effects of attenuation and the total attenuation coefficient in dependence of the X-ray energy E for glass beads (SiO_2), which are used in the experiments.

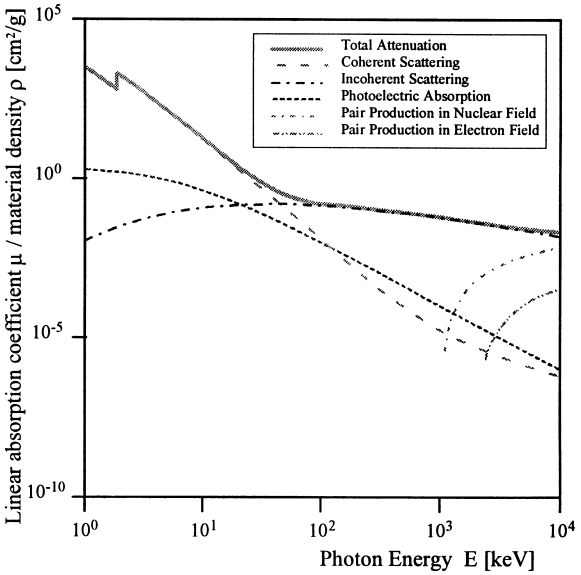

Fig. 2. Processes of attenuation in dependence on X-ray energy E for glass beads [18].

For the installed X-ray source with a maximum energy of 60 keV and glass beads that are irradiated, the main processes of attenuation are the photoelectric effect and coherent and incoherent scattering.

The different effects of X-ray absorption cause, that radiation with lower energy is attenuated better than quanta with higher energy. This leads to a shift of the spectral intensity distribution, if material of different thickness is irradiated. This effect of beam hardening is shown in Fig. 3, where different layers of aluminum are penetrated by X-rays. This example shows, that transmissions measurements with X-rays have to be calibrated.

2.3. Tomographic measuring equipment

The X-ray computer tomography system used mainly consists of a 60 keV X-ray source with an angle of illumination

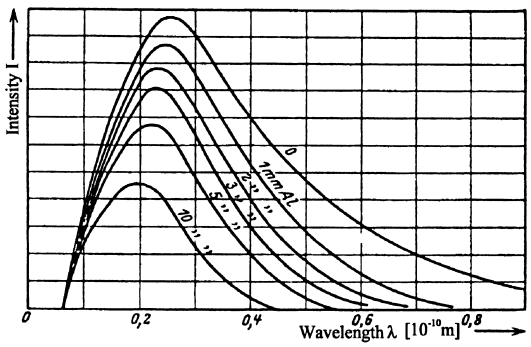

Fig. 3. X-ray hardening caused by different layers of aluminum [15].

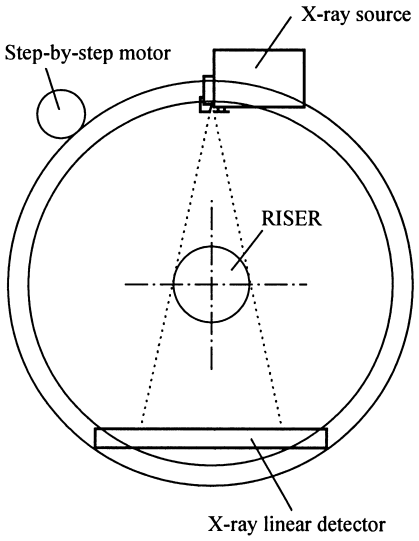

Fig. 4. Scheme of the X-ray computer tomography system.

of ca. 35° and an X-ray linear detector with 1024 sensitive elements and signal resolution of 8 bit. Both components are mounted on a stainless-steel ring, which is rotated with the support of a step-by-step motor. Fig. 4 shows a scheme of the tomographic system that has been applied to the two different circulating fluidized beds.

The principle of transmission tomography measurements with a radiation source producing a fan beam is pictured in Fig. 5. The tube of the circulating fluidized bed is irradiated by fan beams from two different directions in one particular plane. The values of transmission I_1 and I_2 represent the integral value of solids concentration along the approximately linear X-ray beams measured by each of the sensitive elements of the linear detector. Solids inside the reactor causes additional attenuation in comparison to the empty tube and the values of transmission decrease, which is shown for a simple particle in Fig. 5.

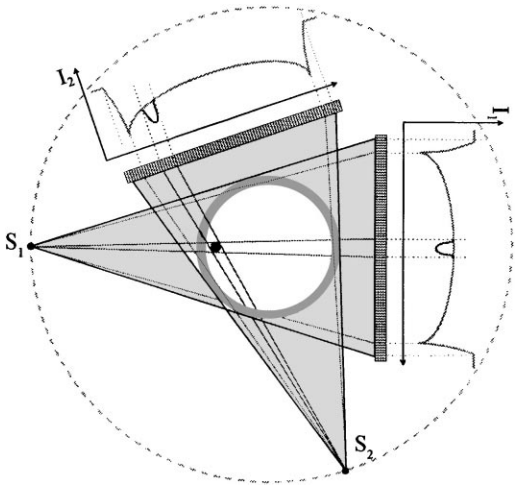

Fig. 5. Principle of tomographic measurements.

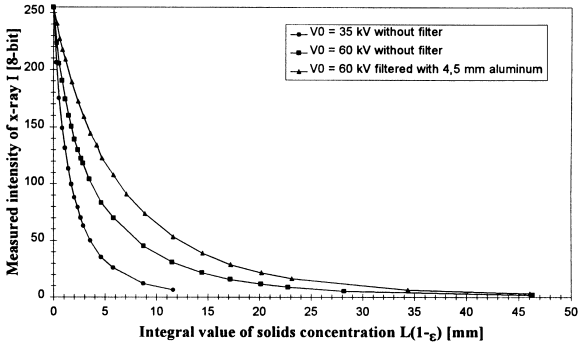

Fig. 6. Calibration of the X-ray computer tomography system.

Each of approximately linear X-ray beams is following Beer's Law (Eq. (5)). So it is possible to calculate the average solids concentration $(1-\varepsilon)$ along one path of the X-ray beam s from measured values of transmission with and without a gas–solids flow inside the tube, respectively I and I_0:

$$(1-\varepsilon) = \frac{1}{\int \mu(s)\mathrm{d}s} \ln \frac{I_0}{I} \tag{5}$$

The attenuation due to the gas can be neglected in comparison to the solids. As shown above, the linear absorption coefficient μ is influenced by a number of different variables and therefore it is a function of the beam coordinate s. To calculate average solids concentration according to Eq. (5), a calibration for the whole system is necessary.

Fig. 6 shows measured intensities of the linear detector I for different integral values of solids concentration $L(1-\varepsilon)$, which have been obtained for glass beads with three different intensity distributions of the X-ray source. The intensity distribution was varied by changing the target voltage V_0 applied to the X-ray tube and by using a 4.5 mm aluminum filter to harden radiation.

The three different calibration functions also indicate the operative range of the tomographic system. In order to measure low solids concentrations with an optimum of accuracy for a given length L the target voltage V_0 applied to the X-ray tube should be the minimum possible without using any filter. In our case with a maximum tube diameter of 0.19 m average solids concentrations $(1-\varepsilon)$ from almost 0 up to 3 vol% can be detected with 35 keV applied. Such concentrations are typical for the downflow of a circulating fluidized bed.

The target voltage, V_0, should be increased and radiation should be filtered to measure highest concentrations which usually can be found at the bottom of a circulating fluidized bed. With a target voltage of 60 keV and a 4.5 mm aluminum filter it is possible to use the system for average solids concentrations up to 20 vol% in a 0.19 m tube. However, the problem of applying higher voltage is that accuracy for low concentrations is worse and using filters measuring time increases because of lower radiation intensities.

After an adequate calibration, it is possible to calculate the integral value of solids concentration $L(1-\varepsilon)$ for each

approximately linear beam. To calculate local solids concentrations inside the tube it is necessary to know many integral values $L(1-\varepsilon)$ for a number of different directions. The calculation of local values of solids concentration $(1-\varepsilon)$ is carried out by an ART, which is an iterative algorithm to solve underdeterminated linear equation systems. For industrial applications ART is rather used than, e.g. Fourier inversion or convolutional backprojection, because it shows better results with limited data and it is very easy to incorporate prior knowledge like restrictions in the reconstruction area [11].

For reliable tomographic results it is essential that all X-ray attenuation measurements at each angular position represent the same flow structure inside the reconstruction area. Due to fluctuations of a vertical gas–solids flow it is necessary to increase the measuring time for each angular projection in order to average these fluctuations. As a consequence, only time averaged solids concentrations can be obtained with X-ray computer tomography. One solids concentration profile needs ca. 20–30 min to be measured, depending on the time scale of the fluctuations inside the tube.

However, the main advantage of this technique is the non-intrusive measurement of local solids concentrations even near to the wall of the tube, where other systems like intrusive probes deliver no reliable results because of their large measurement volumes. In addition to that, the spatial resolution of the system is relatively high. The system presented in this paper allows a minimum spatial resolution of 0.2 mm. Finally, X-ray computer tomography is insensitive to electronic charging of the gas–solids flow inside the circulating fluidized, which normally is a great problem especially for very fast measuring techniques like capacitance probes or electrical impedance tomography.

To prove the reliability of the whole tomographic system a cylinder of glass beads covered by an extremely thin layer of latex has been measured (shown in Fig. 7). The mean solids concentration $(1-\varepsilon)_{av}$ was calculated as 59.2 vol%. This academic object was measured with the same parameter of the X-ray tomography system like the results presented later on. After the reconstruction process the solids concentration distribution of the object was averaged to 61.2 vol%. The thin lines outside the cylinder of glass beads are caused by the ART-algorithm and called artifacts.

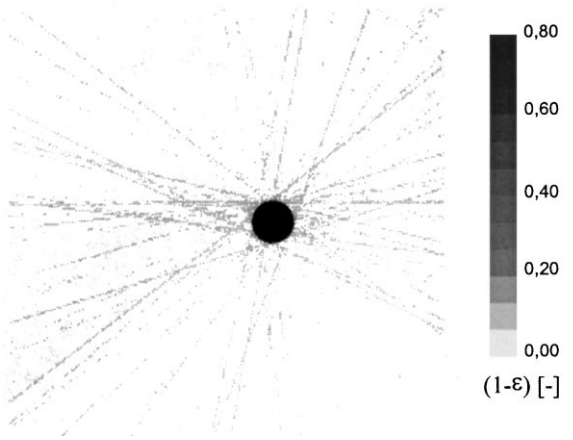

Fig. 7. Reconstruction of a test object made of glass beads.

Also, other experiments with objects of a certain solids concentration distribution show that the relative divergence between the given and the measured value of average solids concentration is maximum 5%. However, the error of local solids concentration may be up to 10%.

3. Experimental setup

The X-ray computer tomography system has been installed at two different kinds of circulating fluidized beds. One plant was built up to investigate the upflow of a circulating fluidized bed with high solids concentrations inside. For the gas–solids flow is moving against the direction of gravity this reactor is called riser. The other plant is used to explain phenomena of the downflow part of a circulating bed and therefore it is termed downer.

Both plants shown in Fig. 8 are special constructions of circulating fluidized beds. To realize a circulating gas–solids flow air is provided by a blower and mixed with solids at the bottom of the plants. Both phases flow against the direction of gravity, vertically upwards. At the end of the upflow tube both phases are quickly and completely separated in cyclones. Segregated solids move downwards through the downer and then through an angled standpipe back into the riser. The gas flow rate through the circulating fluidized beds is measured by orifice meters. At each plants a number of differential pressure transducers are mounted to observe static pressure. The solid flux circulating in the plant can be measured by closing a valve below a hopper and weighing the variation of solid accumulation inside the hopper. In the riser plant, the hopper is inserted at the top of the downflow whereas in the downer plant it is mounted close to the bottom. The main differences between both plants are the position of the gas–solids distributor and the additional solids segregation at the bottom of the downer plant. The riser plant consists of tube elements made of stainless steel with an inner diameter of 0.19 m and a total height of 14 m for the upflow. The downflow of the downer plant is as well made of stainless steel with an inner diameter of 0.15 and 8.5 m total height.

In order to measure the solids distribution inside both plants with the tomographic system four 0.5 m, respectively, 0.25 m long plexiglas tube elements are inserted between the stainless-steel elements. With plexiglas tube elements instead of stainless-steel elements the decrease in intensity only because of tube material is reduced.

Experiments have been carried out with narrowly size-distributed glass beads between 50 and 70 μm, which are ideal spherical and insensitive to breakage and attrition. The riser was operated at superficial gas velocities U_G from 2 to 7 m/s, which leads to solids circulating mass fluxes

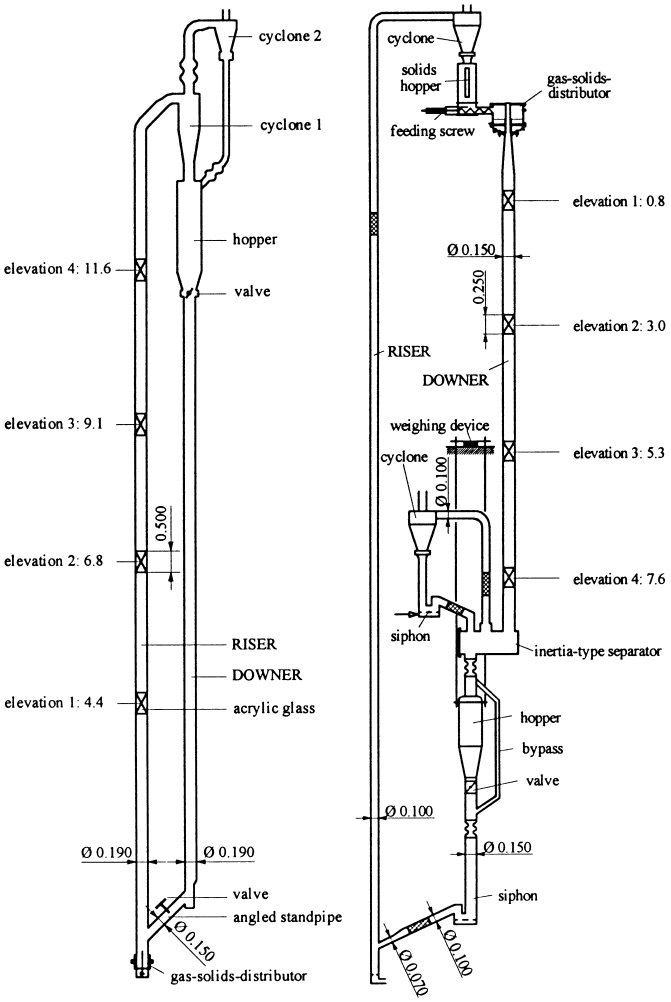

Fig. 8. Sketch of the riser and downer plant.

G_S from 30 up to 600 kg/(m^{2}s) and area weighted solids concentrations $(1-\varepsilon)_{av}$ of 1.8–17.2 vol%. In the downer it is possible to adjust U_G between 0 and 7 m/s so that G_S from 30 up to 100 kg/(m^{2}s) and $(1-\varepsilon)_{av}$ between 0.2 and 2.0 vol% can be obtained.

4. Results and discussion

For the results presented in the paper the radial concentration profiles are reconstructed from 128 angular projections to a 256×256 reconstruction grid according to a spatial resolution of 0.8 mm. At each angular position, the X-ray linear detector is read out 200 times and the results are averaged. This implies an integration time of ca. 15 s for each of the 128 projections and in total a time of 30 min for one radial concentration profile. In Figs. 9 and 10, the tube material shown as an intense black circle is not reconstructed together with solids but inserted afterwards because of different absorption coefficients for plexiglas and glass beads.

4.1. Riser plant

Fig. 9 shows solids concentration distributions measured with the tomographic system at a superficial gas velocity U_G of 2.7 m/s and a specific mass flow rate G_S of 195 kg/(m^{2}s).

All three radial concentration profiles show a parabolic shape with a maximum concentration close to the wall and a minimum concentration in the center of the tube. This typical profile for the upflow in a circulating fluidized leads to solids and gas moving downward in a layer near the wall [19].

The mean value of solids concentration $(1-\varepsilon)_{av}$ over the whole cross section decreases from elevation 1 to elevation 4 (Fig. 8), because of acceleration of gas and solids from the bottom to the top of the riser. At the bottom of the plant local solids concentrations up to 45 vol% are reached near the wall of the tube, which is close to the minimum fluidization

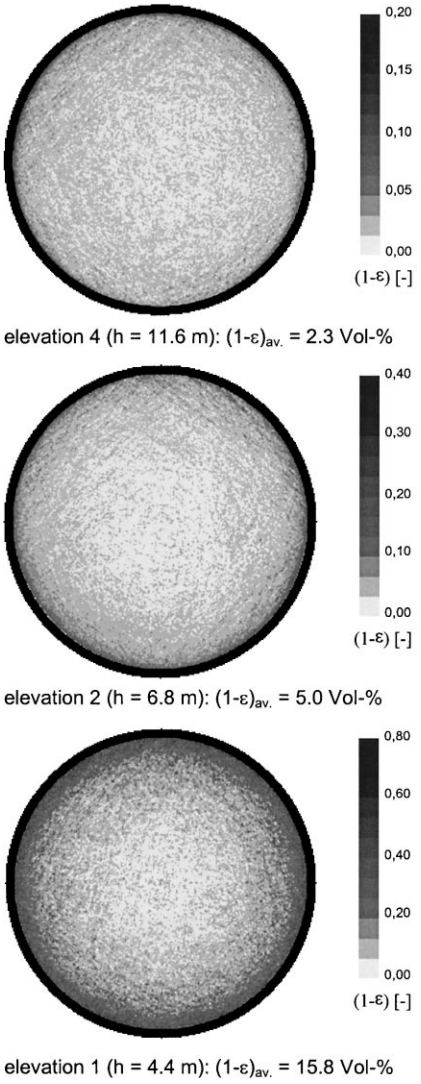

Fig. 9. Solids concentration distribution in the riser ($U_G = 2.7$ m/s, $G_S = 195$ kg/(m^{2}s)).

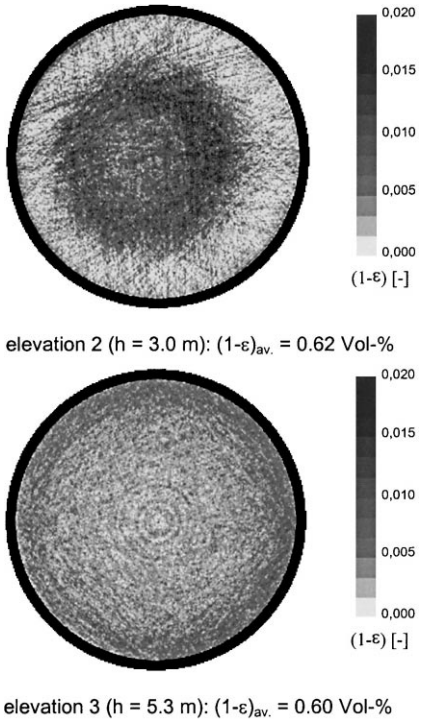

Fig. 10. Solids concentration distribution in the downer ($U_G = 1.3$ m/s, $G_S = 45$ kg/(m^{2}s)).

concentration. It is remarkable that the shape of the solids concentration distribution is similar for all elevations of the riser even at different superficial gas velocities and different circulating mass fluxes.

4.2. Downer plant

Following only one result of the downer plant shall be presented. Fig. 10 shows radial solids concentration distributions obtained by the X-ray computer tomography system occurring at a superficial gas velocity U_G of 1.3 m/s and a circulating mass flux G_S of 45 kg/(m^{2}s).

In comparison to the riser the height h of the downer is given as the distance from the gas–solids distributor, i.e. from the top of the downflow tube to the bottom. Comparing both solids concentration profiles in Fig. 10 a rapid change in the flow structure for different elevations can be observed. At elevation 2, which is closer to the gas–solids distributor, most of the solids are concentrated in the center of the tube, whereas at elevation 3, which is 2.3 m downstream of elevation 2, an almost homogeneous solids concentration distribution is detected. This indicates a strong influence of the gas–solids distributor on the flow patterns inside a downer. Depending on the operating conditions of the gas–solids distributor at the top of the downer various solids concentration distributions can be observed, from a homogeneous distribution over a parabolic profile like in the riser to concentrated strands in the center of the tube.

More details about the flow structures of the downer-reactor described in this paper can be found in Ref. [20]. Comparable results have been also observed by Wang et al. [22].

5. Conclusions

An X-ray computer tomography system consisting of a 60 keV X-ray source and a linear X-ray detector has been developed to study flow structures of circulating fluidized bed. This system shows a lot of advantages in comparison to commonly used measuring techniques like capacitance or optical probes and electrical impedance tomography. Unlike intrusive probes X-ray computed tomography does not influence the flow structure inside the vertical tubes. Moreover, this system is applicable even at higher temperatures or when electric charging caused by flowing particles occurs, because there is no contact to the measuring object.

In addition to that X-ray computer tomography allows a far higher spatial resolution than other systems. If that detailed local information should be obtained by probes a measuring time from 20 to 30 min, necessary for X-ray tomography, is relatively short. However, in comparison to electrical impedance tomography system this acquisition time is still orders of magnitude higher so that snapshots of the flow structure inside circulating fluidized beds are impossible to capture.

After calibrating the system, it is possible to measure average solids concentrations up to 20 vol% and a minimum spatial resolution of 0.2 mm. Testing the tomographic system with well-defined objects shows that results are reliable within an error range of ca. 5%.

Radial solids concentration profiles received both at the upflow and at the downflow of a circulating fluidized bed show the different hydrodynamic properties caused by the direction of gas–solids flow. This knowledge is essential for modeling chemical reactions inside such kind of reactors.

Acknowledgements

Financial support of the experimental investigations by the *Deutsche Forschungsgemeinschaft* (DFG) is gratefully acknowledged.

References

[1] J.R. Grace, A.A. Avidan, T.M. Knowlton, Circulating Fluidized Beds, Blackie Academic and Professional, London, 1997.
[2] A.S. Issangya, D. Rai, J.R. Grace, K.S. Lim, Flow behavior in the riser of a high-density circulating fluidized bed, AIChE Symposium Series No. 317 93 (1998) 25–30.
[3] M.G. Schnitzlein, H. Weinstein, Design parameters determining solid hold-up in fast fluidized bed system, in: P. Basu, J.F. Large (Eds.), Circulating Fluidized Bed Technology II, Pergamon Press, New York, 1988, pp. 205–211.

[4] J.G. Yates, J.R. Simons, Experimental methods in fluidization research, Int. J. Multiphase Flow 20 (1994) 297–330.
[5] H. Weinstein, H.J. Feindt, L. Chen, R.A. Graff, The measurement of turbulence quantities in a high velocity fluidized bed, in: O.E. Potter, D.J. Nicklin (Eds.), Fluidization VII, Engineering Foundation, New York, 1992, pp. 305–312.
[6] J.G. Yates, D.J. Cheesman, Dispersion of gas from coaxial nozzels in a fluidized bed, in: O.E. Potter, D.J. Nicklin (Eds.), Fluidization VII, Engineering Foundation, New York, 1992, pp. 185–192.
[7] J. Chaouki, F. Larachi, M.P. Dudukovic (Eds.), Non-Invasive Monitoring of Multiphase Flows, Elsevier, Amsterdam, 1997.
[8] D.M. Scott, R.A. Williams (Eds.), Frontiers in Industrial Process Tomography, Engineering Foundation, New York, 1996.
[9] D. Toye, P. Marchot, M. Crine, A.-M. Pelsser, G. L'Homme, Local measurement of void fraction and liquid holdup in packed columns using X-ray computed tomography, Chem. Eng. Process. 37 (6) (1998) 511–520.
[10] P. Marchot, M. Crine, G. L'Homme, Rational description of trickle flow through packed beds, Chem. Eng. J. 48 (1) (1992) 49–70.
[11] R.A. Williams, C.-G. Xie, Tomographic techniques for characterizing particulate processes, Part. Syst. Charact. 10 (1993) 252–261.
[12] R. Gordon, A tutorial on ART, IEEE Trans. Nucl. Sci. 21 (1974) 78–93.
[13] G.T. Herman, A. Lent, S.W. Rowland, ART: mathematics and applications, J. Theor. Biol. 42 (1973) 1–32.
[14] J. F. Mulligan, Introductory College Physics, McGraw-Hill Book Company, New York, 1985.
[15] W. Minder, A. Liechti, Röntgenphysik, Springer, Wien, 1955.
[16] E. Hering, Physik für Ingenieure, VDI-Verlag, Düsseldorf, 1992.
[17] H. Morneburg (Ed.), Bildgebende Systeme für die medizinische Diagnostik, Publicis MCD Verlag, München, 1995.
[18] J.H. Hubbell: XCOM: Photo Cross Section Data-base, http://www.physics.nist.gov, 1999.
[19] F. Berruti, J. Chaouki, L. Godfroy, T.S. Pugsley, G.S. Patience, Hydrodynamics of circulating fluidized bed risers: a review, Can. J. Chem. Eng. 73 (1995) 579–602.
[20] P. Lehner, K.-E. Wirth, Effects of the gas/solids distributor on the local and overal solids distribution in a downer reactor, Can. J. Chem. Eng. 77 (1999) 199–206.
[21] T. Dyakowski, R.B. Edwards, C.G. Xie, R.A. Williams, Application of capacitance tomography to gas–solids flows, Chem. Eng. Sci. 52 (13) (1997) 2099–2110.
[22] S.J. Wang, D. Geldart, M.S. Beck, T. Dyakowski, A Behaviour of a Catalyst Powder Flowing Down a Dipleg, Proceedings of 1st World Congress on Industrial Process Tomography, Buxton (GB), pp. 147–152.